



**NAVAL  
POSTGRADUATE  
SCHOOL**

**MONTEREY, CALIFORNIA**

**THESIS**

**SENSIBLE HEAT FLUX RELATED TO VARIATIONS IN  
ATMOSPHERIC TURBULENCE KINETIC ENERGY ON  
A SANDY BEACH**

by

Jessica S. Koscinski

June 2017

Thesis Advisor:  
Second Reader:

Jamie MacMahan  
Qing Wang

**Approved for public release. Distribution is unlimited.**

THIS PAGE INTENTIONALLY LEFT BLANK

REPORT DOCUMENTATION PAGE			Form Approved OMB No. 0704-0188	
Public reporting burden for this collection of information is estimated to average 1 hour per response, including the time for reviewing instruction, searching existing data sources, gathering and maintaining the data needed, and completing and reviewing the collection of information. Send comments regarding this burden estimate or any other aspect of this collection of information, including suggestions for reducing this burden, to Washington headquarters Services, Directorate for Information Operations and Reports, 1215 Jefferson Davis Highway, Suite 1204, Arlington, VA 22202-4302, and to the Office of Management and Budget, Paperwork Reduction Project (0704-0188) Washington, DC 20503.				
1. AGENCY USE ONLY (Leave blank)	2. REPORT DATE June 2017	3. REPORT TYPE AND DATES COVERED Master's thesis		
4. TITLE AND SUBTITLE SENSIBLE HEAT FLUX RELATED TO VARIATIONS IN ATMOSPHERIC TURBULENCE KINETIC ENERGY ON A SANDY BEACH			5. FUNDING NUMBERS	
6. AUTHOR(S) Jessica S. Koscinski				
7. PERFORMING ORGANIZATION NAME(S) AND ADDRESS(ES) Naval Postgraduate School Monterey, CA 93943-5000			8. PERFORMING ORGANIZATION REPORT NUMBER	
9. SPONSORING /MONITORING AGENCY NAME(S) AND ADDRESS(ES) N/A			10. SPONSORING / MONITORING AGENCY REPORT NUMBER	
11. SUPPLEMENTARY NOTES The views expressed in this thesis are those of the author and do not reflect the official policy or position of the Department of Defense or the U.S. Government. IRB number ____N/A____.				
12a. DISTRIBUTION / AVAILABILITY STATEMENT Approved for public release. Distribution is unlimited.			12b. DISTRIBUTION CODE	
13. ABSTRACT (maximum 200 words)  Two field experiments were conducted in the surf zone of the Monterey Bay to explore the relationship between surf zone sea spray and sensible heat flux. Nine flux tripod towers with instrumentation designed to measure atmospheric wind speed and direction, temperature and relative humidity, as well as thermistor and pressure sensors in the surf zone, were deployed throughout the two experiments. Data analysis showed that the ocean temperature was warmer than the air temperature and the environment was mildly unstable throughout most of the two experiments. The total data set was broken into 15-minute averages and limited to onshore winds over 3m/s and a stability range of $-5 < \zeta < 0.5$ , $\zeta$ being the non-dimensional height under Monin-Obukhov Similarity Theory. Sensible heat flux was calculated using the eddy covariance method and also using the COARE 3.5 model, validated for the open ocean, and the results were compared. The model under-predicted measured results by over 50%. Sea spray sensible heat was then calculated and added to the model results; the new comparison showed that the model was nearly the same as the measured results with sea spray sensible heat added.				
14. SUBJECT TERMS Sensible heat flux, turbulence kinetic energy, surf zone			15. NUMBER OF PAGES 57	
			16. PRICE CODE	
17. SECURITY CLASSIFICATION OF REPORT Unclassified	18. SECURITY CLASSIFICATION OF THIS PAGE Unclassified	19. SECURITY CLASSIFICATION OF ABSTRACT Unclassified	20. LIMITATION OF ABSTRACT UU	

THIS PAGE INTENTIONALLY LEFT BLANK

**Approved for public release. Distribution is unlimited.**

**SENSIBLE HEAT FLUX RELATED TO VARIATIONS IN ATMOSPHERIC  
TURBULENCE KINETIC ENERGY ON A SANDY BEACH**

Jessica S. Kosciński  
Lieutenant Commander, United States Navy  
B.A., Buffalo State College, 2005

Submitted in partial fulfillment of the  
requirements for the degree of

**MASTER OF SCIENCE IN METEOROLOGY AND  
PHYSICAL OCEANOGRAPHY**

from the

**NAVAL POSTGRADUATE SCHOOL  
June 2017**

Approved by:        Jamie MacMahan  
                              Thesis Advisor

Qing Wang  
Second Reader

Peter Chu  
Chair, Department of Oceanography

THIS PAGE INTENTIONALLY LEFT BLANK

## ABSTRACT

Two field experiments were conducted in the surf zone of the Monterey Bay to explore the relationship between surf zone sea spray and sensible heat flux. Nine flux tripod towers with instrumentation designed to measure atmospheric wind speed and direction, temperature and relative humidity, as well as thermistor and pressure sensors in the surf zone, were deployed throughout the two experiments. Data analysis showed that the ocean temperature was warmer than the air temperature and the environment was mildly unstable throughout most of the two experiments. The total data set was broken into 15-minute averages and limited to onshore winds over 3 m/s and a stability range of  $-5 < \zeta < 0.5$ ,  $\zeta$  being the non-dimensional height under Monin-Obukhov Similarity Theory. Sensible heat flux was calculated using the eddy covariance method and also using the COARE 3.5 model, validated for the open ocean, and the results were compared. The model under-predicted measured results by over 50%. Sea spray sensible heat was then calculated and added to the model results; the new comparison showed that the model was nearly the same as the measured results with sea spray sensible heat added.

THIS PAGE INTENTIONALLY LEFT BLANK

# TABLE OF CONTENTS

<b>I.</b>	<b>INTRODUCTION.....</b>	<b>1</b>
<b>II.</b>	<b>THEORETICAL BACKGROUND .....</b>	<b>9</b>
	<b>A. REYNOLDS NUMBER.....</b>	<b>9</b>
	<b>B. MONIN-OBUKHOV SIMILARITY THEORY .....</b>	<b>9</b>
	<b>C. DRAG COEFFICIENT .....</b>	<b>10</b>
	<b>D. FOOTPRINT ANALYSIS.....</b>	<b>11</b>
<b>III.</b>	<b>METHODS .....</b>	<b>13</b>
	<b>A. EXPERIMENTAL LOCATIONS.....</b>	<b>13</b>
	<b>B. INSTRUMENTATION .....</b>	<b>14</b>
	<b>C. DATA PROCESSING .....</b>	<b>17</b>
<b>IV.</b>	<b>RESULTS .....</b>	<b>19</b>
	<b>A. ENVIRONMENT.....</b>	<b>19</b>
	<b>B. ROUGHNESS .....</b>	<b>22</b>
	<b>C. STABILITY.....</b>	<b>23</b>
	<b>D. FOOTPRINT.....</b>	<b>25</b>
	<b>E. TURBULENCE KINETIC ENERGY .....</b>	<b>26</b>
	<b>F. SENSIBLE HEAT FLUX.....</b>	<b>29</b>
<b>V.</b>	<b>SUMMARY AND CONCLUSIONS .....</b>	<b>33</b>
	<b>LIST OF REFERENCES.....</b>	<b>35</b>
	<b>INITIAL DISTRIBUTION LIST .....</b>	<b>39</b>

THIS PAGE INTENTIONALLY LEFT BLANK

## LIST OF FIGURES

Figure 1.	Normalized TKE Budget Terms. Source: Garratt (1992).....	7
Figure 2.	Drag Coefficient. Source: Shabani et al. (2016).....	11
Figure 3.	Experimental Locations .....	13
Figure 4.	Instruments and Tower Setup during the October Experiment .....	15
Figure 5.	Wind Speed vs. Direction .....	19
Figure 6.	Hourly Wind Speed and Air Temperature .....	20
Figure 7.	Air-Ocean Temperature Difference .....	21
Figure 8.	Roughness Reynolds Number.....	22
Figure 9.	Thermal Stability .....	24
Figure 10.	Footprint Analysis.....	25
Figure 11.	The Terms of the TKE Budget.....	27
Figure 12.	Zonally separated Buoyancy Flux .....	28
Figure 13.	Contributions of Sand, Surf Zone and Ocean outside Surf Zone .....	28
Figure 14.	Sensible Heat Flux .....	30
Figure 15.	Sensible Heat Flux from October Experiment.....	31
Figure 16.	Sensible Heat Flux from CLASI Experiment .....	32

THIS PAGE INTENTIONALLY LEFT BLANK

## LIST OF TABLES

Table 1.	Instrumentation for October Deployment.....	16
Table 2.	Instrumentation for CLASI Deployment .....	16

THIS PAGE INTENTIONALLY LEFT BLANK

## **LIST OF ACRONYMS AND ABBREVIATIONS**

CLASI	Coastal Land-Air-Sea-Interaction
DMB	Del Monte Beach
ESN	Elkhorn Slough North
ESS	Elkhorn Slough South
MAB	Manaresa Beach
MAR	Marina Beach
MOST	Monin-Obukhov Similarity Theory
RSMAS	Rosenstiel School of Marine and Atmospheric Science
SHF	sensible heat flux
TKE	turbulence kinetic energy

THIS PAGE INTENTIONALLY LEFT BLANK

## **ACKNOWLEDGMENTS**

I would like to thank my thesis advisor, Jamie MacMahan, whose knowledge, motivation and assistance made this possible. Thank you also to Qing Wang, my second reader, an air-sea expert, and Ed Thornton, a legend in the field of nearshore and my third set of eyes. To LCDR Darin Keeter, who got me started on this path and who has been a friend and mentor, thank you. Thanks to my cohort, Adam, Andrew, Chris A., Chris B., Eric and Kevin. I wouldn't have made it through these two and a half years without you. Finally, thank you, Tucker, for always having time during your busy Ph.D. process to help me with whatever MATLAB problem or stupid question I had.

THIS PAGE INTENTIONALLY LEFT BLANK

# I. INTRODUCTION

Atmospheric and oceanic factors in the littoral region are of increasing importance to the U.S. Navy. The “littoral” in simple definition, refers to a coastal region or a shore and geographically it is a coastline zone between extreme high and low tides (Vego 2014). Two of the primary anti-access/area-denial capabilities in the littorals are land-based aircraft and unmanned aerial vehicles. One advantage of using these platforms in the littorals is the enhanced probability of avoiding detection and achieving surprise if they approach targets at low altitudes or over land (Vego 2014). Another example of a need for atmospheric data in the littorals is the occurrence of atmospheric ducting. Ducting can trap electromagnetic energy and can both prevent it from reaching a sensor and allow it to travel farther than had it not been in a duct. Ducting occurs in conditions of temperature and water vapor vertical gradients such as in the littorals where large diurnal land/sea temperature differences are common (Vego 2014). Unfortunately current numerical models, such as the Coupled Ocean/Atmosphere Mesoscale Prediction System (COAMPS) run at the Naval Research Laboratory in Monterey, California, struggle with modeling land/ocean boundaries. The nearshore processes that influence those boundaries are not well parameterized because of insufficient data in coastal areas including the surf zone. To mitigate shortfalls, the Office of Naval Research provided funding for research into the nearshore processes that might improve numerical modeling. The goal of this thesis is to show that there are differences in the magnitude of sensible heat flux and turbulence kinetic energy (TKE) in the surf zone as compared to the open ocean. Measurements of wind speed and direction as well as air and ocean temperature are used to determine those differences.

In the marine environment, sensible heat is transferred from the water to the atmosphere when the ocean is warmer than the air above it. Sensible heat flux is driven by wind speed and air-sea temperature differences and was defined by Andreas (1992) as:

$$H_s = \rho_a C_p C_{H10} U_{10} (T_w - T_a), \quad (1)$$

where  $\rho_a$  is air density in  $\text{kg/m}^3$ ,  $C_p$  is specific heat of air in  $\text{kJ/kg}\cdot^\circ\text{C}$ ,  $U_{10}$  is the 10 m wind speed in m/s,  $T_w$  is sea surface temperature and  $T_a$  is 10 m air temperature in  $^\circ\text{C}$  and  $C_{H10}$  is the transfer coefficient for sensible heat where:

$$C_{H10} = \frac{C_{HN10} (C_{D10} / C_{DN10})^{1/2}}{1 - k^{-1} C_{HN10} C_{DN10}^{-1/2} \psi_h(10/L)}, \quad (2)$$

where  $C_{H10}$ ,  $C_{D10}$ , and  $C_{E10}$  are bulk transfer coefficients for momentum with subscripted  $N$  denoting neutral stability,  $k = 0.4$  is the von Kármán constant,  $L$  is the Obukhov length in meters, and  $\psi_h(10/L) = 2 \ln[(1 + ([1 - 16(10/L)]^{1/4})^2) / 2]$  is a stability correction (Andreas 1992). Latent heat flux contributes to the overall heat flux and is defined as:

$$H_L = L_v C_{E10} U_{10} (\rho_{vs} - \rho_{va}), \quad (3)$$

where  $L_v = 2,260$  kJ/kg is the latent heat of vaporization of water,  $\rho_{vs}$  is water vapor density of air in equilibrium with sea water and  $\rho_{va}$  is water vapor density of the air (Andreas 1992).

Sensible heat flux over the open ocean has been studied for decades, starting with Pond et al. (1971), who collected data from the M/V Flip and determined that sensible heat flux was a small part of the total heat flux at a fixed value of  $1.3 \text{ mW cm}^{-2}$ . Mahrt et al. (2012), recently measured sensible heat flux values of up to  $60 \text{ W m}^{-2}$  for winds over  $20 \text{ ms}^{-1}$  and up to  $20 \text{ W m}^{-2}$  for high winds, even in near-neutral conditions.

The production of sea spray adds an additional layer of sensible heat transfer to the atmosphere as aerosols are expelled into the air at the temperature of the ocean surface. These aerosols are able to release their sensible heat into the atmosphere to the point of equilibrium and reenter the ocean before evaporating (Mahrt et al. 2012). Wave energy dissipation and wind speed contribute directly to the generation and transport of sea spray. The primary means of aerosol generation is wave breaking (Neele et al. 1998, Van Eijk et al. 2011). It was shown that the aerosol emission from a coastal wave-breaking zone can be reasonably predicted, and that there is a simple relationship involving wave energy dissipation and the amount of aerosol produced (Chomka and Petelski 1997). Wind provides the means of transport of aerosols away from the origin of

generation (Neele et al. 1998, De Leeuw et al. 2000, Van Eijk et al. 2006, Andreas et al. 2015, Andreas 2016).

For wave breaking in the surf zone, Andreas (2016) measured spray concentrations on a rocky shore that were 2–3 orders of magnitude larger than concentrations found in the open ocean for droplets smaller than  $30\mu\text{m}$ . This is largely because a contributor to sea spray aerosols in the surf zone is white water, that is, water that has been aerated and roughened into froth by mechanical processes. White water coverage is ubiquitous in the surf zone which includes breaking waves, more so than in the open ocean where white caps are the primary source of white water (Andreas 2016). Andreas (2016) surmised that the concentration of aerosol spray he was recording came from the surf zone and not from the waves crashing on the rocks because the rocky area was outside of the footprint region. Near surface aerosol concentrations ( $C_0$ ) found in this experiment for wind speeds of  $6\text{--}10\text{m/s}$  and for droplet sizes of  $\sim 1\text{--}100\mu\text{m}$  were from  $\sim 10^5\text{m}^{-3}\mu\text{m}^{-1}$ , for smaller droplets, to  $\sim 10^2\text{m}^{-3}\mu\text{m}^{-1}$ , for the largest droplets. For this calculation of nearshore aerosol concentrations:

$$C_0(r_0) = C(z, r_0) \left( \frac{A_{1/3}}{z} \right)^{-\eta_g(r_0)/(kz + f_s)}, \quad (4)$$

where  $C$  is the measured aerosol concentration at height  $z$  above mean sea level,  $r_0$  is the initial radius of the droplet,  $A_{1/3} = H_{1/3}/2$  is the significant wave amplitude and is half of the significant wave height ( $H_{1/3}$ ),  $\eta_g(r_0)$  is the terminal fall speed of the droplet,  $u_* = (\overline{w'u'^2} + \overline{w'v'^2})^{1/4}$  is the frictional velocity, and  $f_s$  is related to the turbulent diffusivity of the droplets given by:

$$f_s(r_0, u_*) = \frac{1}{1 + 2[\eta_g(r_0)/\sigma_w]^2}, \quad (5)$$

where  $\sigma_w$  is the standard deviation of the vertical velocity fluctuations of the air (Andreas 2016). Similar results were described by de Leeuw et al. (2000) who reported a

surf zone aerosol size distribution of  $0.16-47\mu\text{m}$  and from modeled results by Neele et al. (1998) who reported surf produced aerosol flux values of  $\sim 10^4 \text{m}^{-3} \mu\text{m}^{-1}$ .

Once the concentration of aerosols in an area of interest is known, the sensible and latent heat exchange with the atmosphere can be calculated as:

$$H_{s,sp} = \rho_w c_{ps} (T_w - T_{eq}) [1 - \exp(-\tau_f / \tau_T)] \left( \frac{4}{3} \pi r_0^3 \frac{dF}{dr_0} \right) \quad (6)$$

and

$$H_{L,sp} = \rho_w L_v \left\{ 1 - \left[ \frac{r(\tau_f)}{r_0} \right]^3 \right\} \left( \frac{4\pi r_0^3}{3} \frac{dF}{dr_0} \right), \quad (7)$$

where  $\rho_w$  is water density,  $c_{ps}$  is the specific heat of sea water,  $T_{eq}$  is the temperature of a saline droplet when it reaches equilibrium, with the atmosphere,  $\tau_f = \frac{A_{1/3}}{\eta_g(r_0)}$  is the time required for a droplet to fall a certain distance in still air, and  $\tau_T$  is the time for a droplet to undergo 63% of its potential temperature change. It is assumed that  $\tau_f \gg \tau_T$  for droplets with initial radii less than 100 to 200  $\mu\text{m}$  for wind speeds up to 20  $\text{ms}^{-1}$  (Andreas 1992).  $\frac{dF}{dr_0}$  in this equation is the sea spray generation function for the open ocean and is calculated as:

$$\frac{dF}{dr_0} = U_{A_{1/3}} C_0(r_0, U_{N10}) \quad (8)$$

with:

$$U_{A_{1/3}} = U + \frac{u_*}{k} \left[ \ln\left(\frac{A_{1/3}}{z}\right) - \Psi_h\left(\frac{A_{1/3}}{L}\right) + \Psi_h\left(\frac{z}{L}\right) \right], \quad (9)$$

where  $U_{N10}$  is the 10 m neutral wind speed, and  $U$  is wind speed (Andreas 2016).

It is noted that  $(\frac{4}{3}\pi r_0^3 / 3)(\frac{dF}{dr})$  is the volume flux spray (Andreas 1992).

De Leeuw et al. (2000) give a sea spray generation function for the surf zone:

$$\left(\frac{dF(r)}{dr}\right)_{surf} = \frac{U}{W} \left(\frac{dN(r)}{dr}\right)_{surf}, \quad (10)$$

where W is the width of the surf zone, and:

$$\left(\frac{dN(r)}{dr}\right)_{surf} = \int_0^{z_{max}} \left(\frac{dN(r,z)}{dr}\right)_{surf} dz \quad (11)$$

is the height integrated size dependent number concentrations of sea spray aerosols produced in the surf zone. They also defined a single equation describing the surf source function for winds up to 9 ms<sup>-1</sup> as  $\frac{dF_N}{dr} = 2.2 \times e^{0.23 \times U_{10}} \times (2r)^{-1.65}$  when applied to particles with diameters between 1.6 and 20 μm (Aubinet et al. 2012). The sensible heat flux can be calculated using the eddy covariance of buoyancy flux as applied to sonic anemometer measurements, as:

$$H_s = \overline{\rho_a c_p w' \theta'_s} = \frac{\overline{p_a \cdot m_a}}{R \cdot \overline{\theta}} \cdot \overline{c_p w' \theta'_s}, \quad (12)$$

where  $\theta'_s$  is the sonic temperature,  $p_a$  is the dry atmospheric pressure, R is the universal gas constant, and  $m_a$  is the dry air molar mass. Buoyancy flux can also be measured using vertical profiles of wind speed and temperature (e.g., Akylas and Tombrou 2005).

A more practical way to determine buoyancy flux is through use of the TKE budget. TKE can be separated into the forces that are sources or sinks of turbulence including buoyancy flux, shear production, turbulent transport by pressure fluctuations, dissipation and flux divergence. The TKE budget as explained by Srivastava and Sarthi (2002) is:

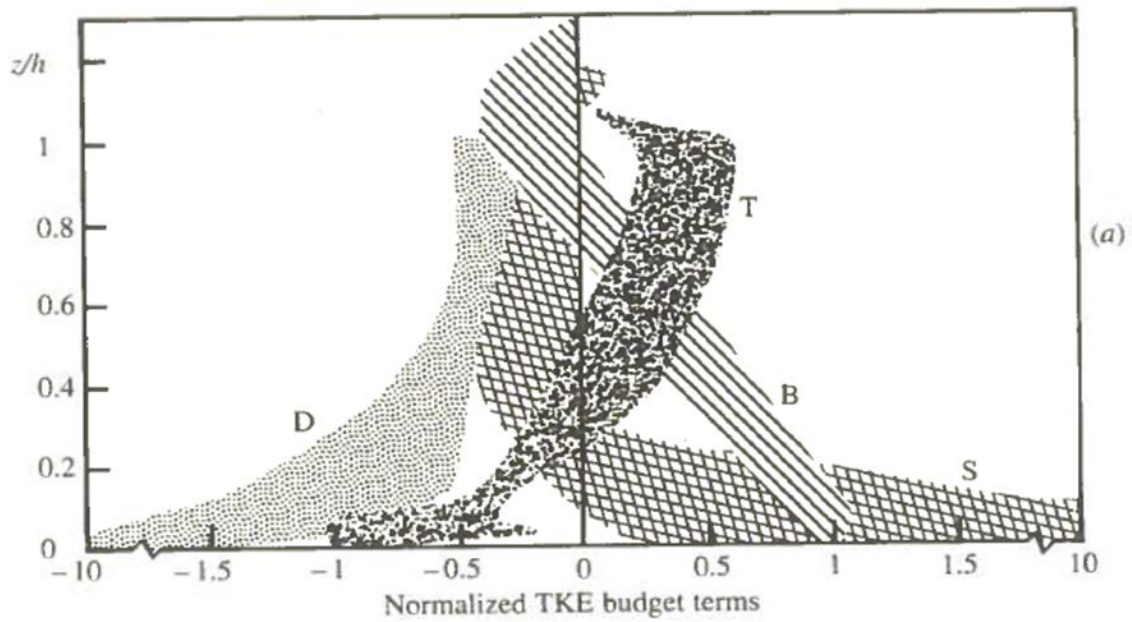
$$\begin{array}{cccc} \frac{g}{\theta_v} \overline{(w' \theta'_v)} & - \overline{w' u'} \frac{\partial \overline{u}}{\partial z} & - \frac{\partial \overline{(w' e)}}{\partial z} & - \varepsilon = 0, \\ \uparrow & \uparrow & \uparrow & \uparrow \\ \text{Term 1} & \text{Term 2} & \text{Term 3} & \text{Term 4} \end{array} \quad (13)$$

where  $\mathbf{g}$  is the acceleration of gravity,  $\theta_v$  is the virtual potential temperature,  $\mathbf{u}$ ,  $\mathbf{v}$  and  $\mathbf{w}$  are the horizontal and vertical components of the wind, and primes denote perturbation from the mean, denoted by an over bar,  $Z$  is height above the surface,  $\varepsilon$  is the dissipation and  $\bar{e} = \frac{1}{2}(\overline{u'^2} + \overline{v'^2} + \overline{w'^2})$  is the total TKE.

Term 1 is the buoyancy flux, which describes the tendency of an air parcel to move vertically in response to its density difference from its surrounding environment. Term 2, the shear production, describes the mechanical generation of turbulence. Term 3 is flux divergence, which describes the differential transport of TKE by turbulent eddies. Term 4, dissipation, is a sink that reduces turbulence. Pressure transport,  $-\frac{\overline{\partial w' p' / \rho_0}}{\partial z}$  is omitted from this budget, as it is known to be very difficult to measure directly (Nilsson et al. 2015). Equation (13) also assumes stationary and horizontal homogeneity of the mean and TKE fields.

Terms in the TKE budget take precedence based on the stability of the atmosphere. The accepted scheme as introduced by Garratt (1992) shows that 1) in the neutral near surface and stable cases, shear production balances dissipation; 2) in the unstable case, in the mid to upper boundary layer, TKE is maintained by the combination of turbulence and pressure transport (see Figure 1).

*Turbulent kinetic energy and stability parameters*



Terms in the TKE budget as a function of height, normalized in the case of the clear daytime ABL. Profiles based on observations and model simulations. B is the buoyancy term, D is dissipation, S is shear generation, and T is the Transport term.

Figure 1. Normalized TKE Budget Terms. Source: Garratt (1992).

THIS PAGE INTENTIONALLY LEFT BLANK

## II. THEORETICAL BACKGROUND

### A. REYNOLDS NUMBER

A first order determination of the likelihood of turbulence involves looking at the general flow of the air in the footprint area. The Reynolds Number is a ratio of the inertial force ( $-U^2/L$ ) to the viscous force ( $-\nu U/L^2$ ) where  $\nu$  is the kinematic viscosity and  $Re = UL/\nu$ . A fluid is capable of developing turbulence when the Reynolds Number is large, i.e., when the inertial term overwhelmingly dominates the viscous term (American Meteorological Society 2012). Expanding on this idea, the Roughness Reynolds number  $R_* = \frac{z_0 u_*}{\nu}$  describes the roughness of the airflow at the boundary where  $z_0$  is the surface roughness. Over the ocean,  $z_0$  can be described by the Charnock relation  $z_0 = \frac{\alpha u_*^2}{g}$ ,  $\alpha$  being the Charnock parameter,  $0.01 \leq \alpha \leq 0.02$  (Andreas 2012).

### B. MONIN-OBUKHOV SIMILARITY THEORY

The Monin-Obukhov Similarity Theory (MOST), developed by A.S. Monin and V. M. Obukhov in 1954, describes turbulent vertical fluxes and how they are related to the mean profiles in the atmospheric surface layer (Akylas and Tombrou 2005). The atmospheric surface layer, as defined in MOST, is the bottom of the boundary layer where surface turbulent fluxes and stress vary by less than 10% of their magnitude (Stull 1988). The theory states that atmospheric stability is defined as  $\zeta = \frac{z}{L}$  where  $z$  is the height above the surface, much less than the height of the boundary layer, and  $L$  is the Obukhov length, given by  $L = \frac{-u_*^3 T_v}{kgw'\theta_v}$  where  $T_v$  is the virtual temperature (Akylas and Tombrou 2005). Experimental results show that while MOST fits experimental data well at or near neutral conditions ( $\zeta \rightarrow 0$ ), it is not valid in stable ( $\zeta > 0$ ) or very unstable ( $\zeta < -10$ ) conditions (Akylas and Tombrou 2005).

### C. DRAG COEFFICIENT

Using the methods of Andreas et al. (2012) and Vickers et al. (2013), the 10 m neutral wind is calculated by

$$U_{N10} = U - \left(\frac{u_*}{k}\right) \ln(z/10) + \left(\frac{u_*}{k}\right) \Psi_h, \quad (14)$$

where:

$$\Psi_h(\zeta) = 2 \ln\left(\frac{1+x}{2}\right) + \ln\left(\frac{1+x^2}{2}\right) - 2 \tan^{-1}(x) + \pi/2; \quad \zeta < 0 \quad (15)$$

and:

$$\Psi_h(\zeta) = -a_2 \zeta; \quad \zeta > 0, \quad (16)$$

where  $x = (1 - a_1 \zeta)^{1/4}$ ,  $a_1 = 16$ , and  $a_2 = 5$  (Vickers et al. 2013).

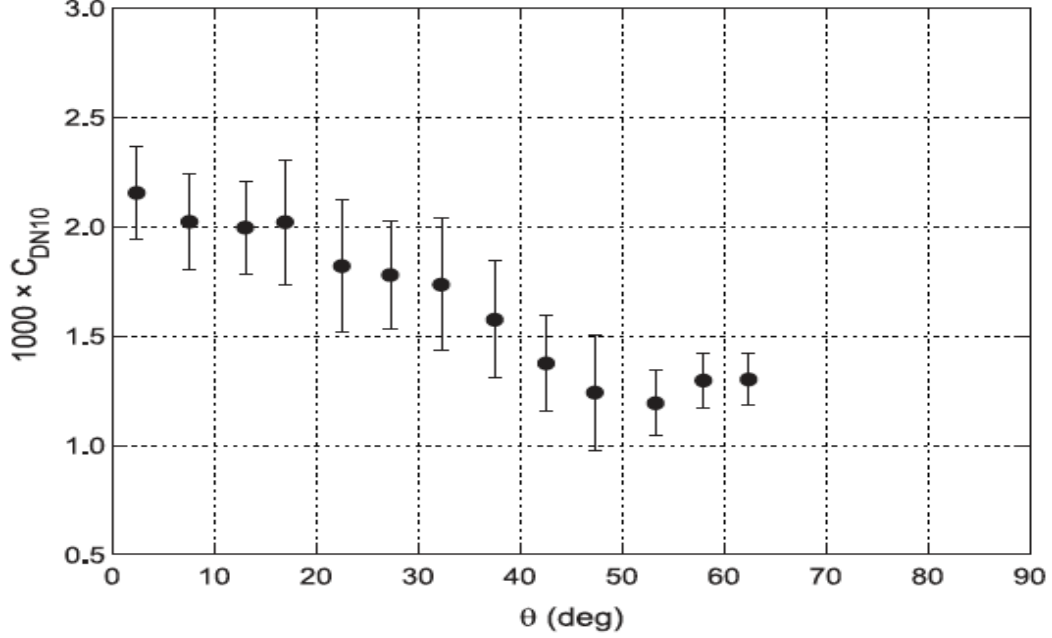
A drag coefficient is often required when relating fluxes to mean properties of the flow at a single level (Garratt 1992) and is a dimensionless ratio of the component of force parallel to the direction of flow exerted on a body by a fluid to the kinetic energy of the fluid multiplied by a characteristic surface area of the body (American Meteorological Society 2012). The neutral drag coefficient is traditionally calculated as

$$C_{DN} = \frac{k^2}{[\ln(z/z_0)]^2}, \quad (17)$$

where  $\zeta = 0$  (Garratt 1992). Using the eddy covariance method, the 10 m neutral drag coefficient was simplified by (Andreas et al. 2012) as:

$$C_{DN10} = \left(\frac{u_*}{U_{N10}}\right)^2. \quad (18)$$

Shabani et al. (2016) noted a well-defined dependence of the wind drag coefficient ( $C_D$ ) on the wind direction where the largest  $C_D$  was found to correspond to onshore winds and the lowest  $C_D$  corresponded to alongshore winds (see Figure 2). Based on his results, it is clear that there must be an understanding of where the instrument's measurements originate.



Measured drag coefficients ( $C_{DN10}$ ), measured at a height of 5m above mean water, vs. the angle ( $\theta$ ) between the wind and wave directions.

Figure 2. Drag Coefficient. Source: Shabani et al. (2016).

#### D. FOOTPRINT ANALYSIS

The footprint area is the field of view of the flux sensor that includes all effective sources and sinks and the footprint is defined as the contribution of all sources and sinks to the measured vertical flux (Aubinet et al. 2012). The footprint function  $\phi$  is contained in the integral equation of diffusion (Aubinet et al. 2012):

$$\gamma = \int_{\mathbb{R}} \phi(\vec{y}, \vec{y}') Q(\vec{y}') d(\vec{y}') , \quad (19)$$

where  $\gamma$  is the quantity being measured at location  $\vec{y}$ , and  $Q(\vec{y}')$  is the source/sink strength in the surface volume  $\mathbb{R}$ .

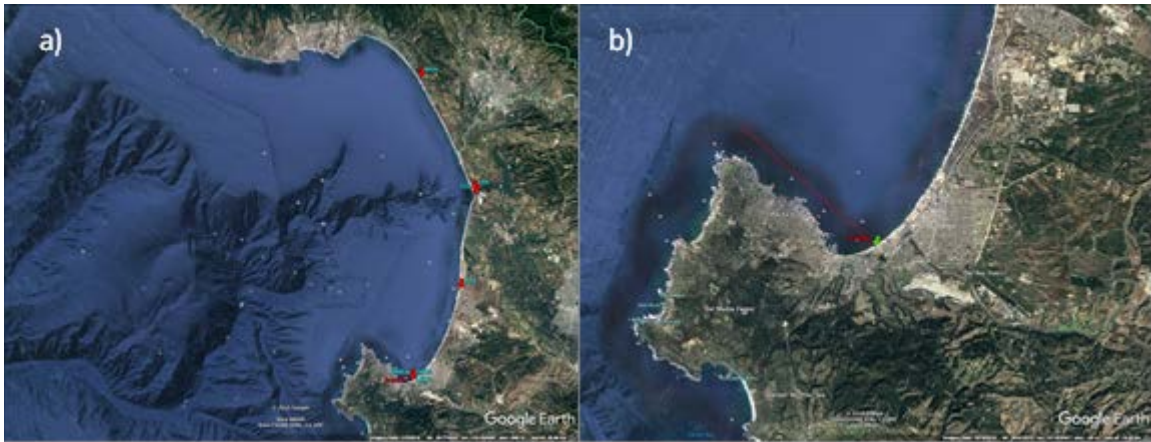
THIS PAGE INTENTIONALLY LEFT BLANK

### III. METHODS

#### A. EXPERIMENTAL LOCATIONS

Field experiments were conducted in the Monterey Bay, which is classified as a Mediterranean environment under the Köppen-Geiger climate classification. More specifically, it is a temperate zone with a warm, dry summer (Peel et al. 2007) where the water temperature is often warmer than the air temperature. The prevailing wind is from the Northwest, and due to the orientation of Monterey Bay, it crosses both ocean water in the harbor, and land (see Figure 3).

The first portion of the experiment was conducted from 2 October to 5 November 2015 on Del Monte Beach in Monterey, California. The site is a sandy beach with moderate to gentle slope and sand dominantly quartz and feldspar, with a medium to fine texture (Hohenstein et al. 1965). The beach lies in the lee of the Monterey peninsula and is protected from southwesterly to westerly waves and swell (see Figure 3).



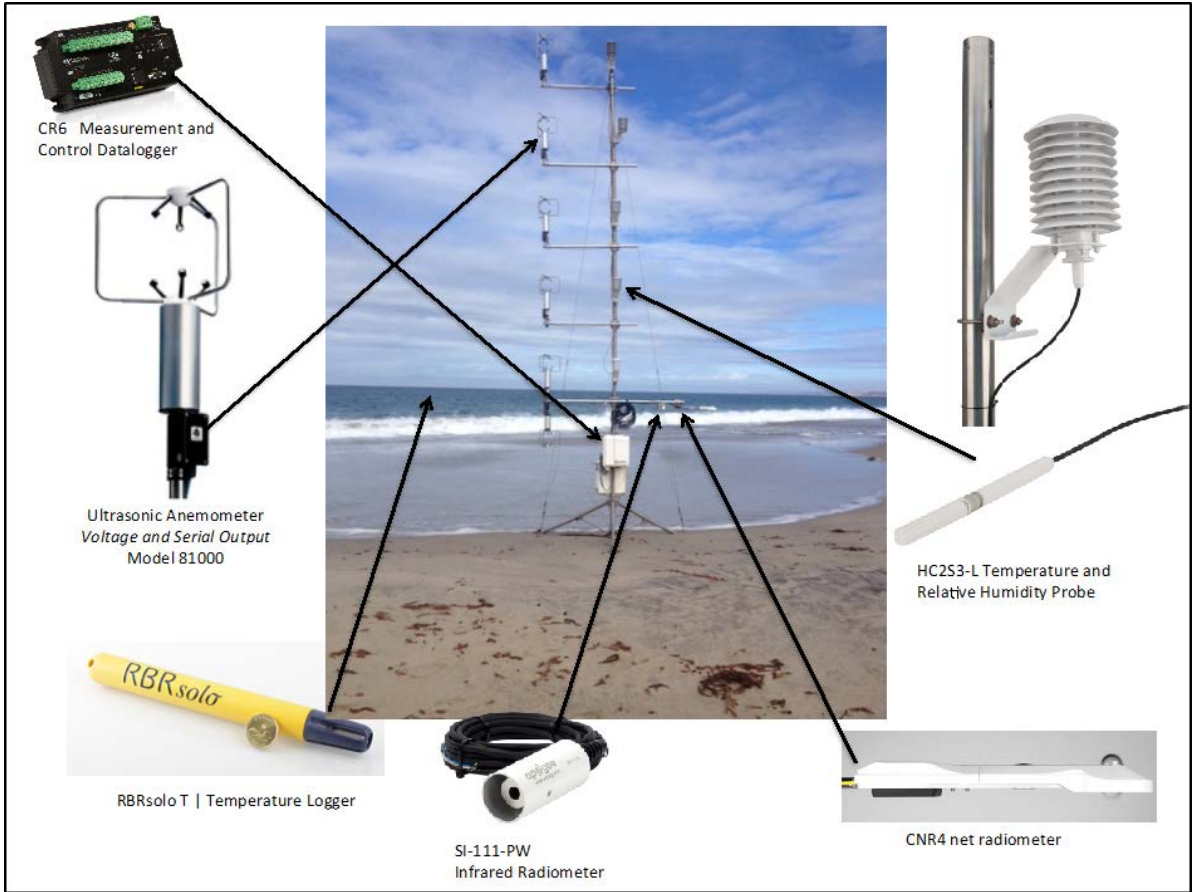
a) Tower locations From: Google Earth. From North to South, Manresa State Beach (MAN), Elkhorn Slough North (ESN), Elkhorn Slough South (ESS), Marina State Beach (MAB), Del Monte Beach (DMB1, DMB2, DMB3, October). b) Prevailing wind direction, North to Northwest ( $315^{\circ}$ T is shown by the red line). Images from Google Earth.

Figure 3. Experimental Locations

The second portion of the experiment was conducted in June 2016 in collaboration with the Rosenstiel School of Marine and Atmospheric Science (RSMAS) as a part of the Coastal Land-Air-Sea Interaction (CLASI) experiment. Four separate locations with different environmental conditions were chosen for this experiment. The northernmost location was Manresa State beach (MAN), which is moderately protected from northwesterly waves and swell by the outcropping of Santa Cruz Peninsula, California (see Figure 3). This is a gently sloping beach with coarse sand, backed by a steep bluff. Two beach sites were located on the middle of Monterey Bay on the north and south sides of Elkhorn Slough (see Figure 3). Elkhorn Slough North (ESN) is a gently sloping beach with medium sand backed by a low dune and moderately shielded from southerly waves and swell by a jetty, not shown. Elkhorn Slough South (ESS) is a gently sloping beach with medium sand and is not significantly blocked in any direction. Further to the South, Marina State beach (MAB) and Del Monte Beach (DMB) are located in southern Monterey Bay (see Figure 3). MAB has a steeply sloping beach with medium to coarse sand and is backed by a steep dune.

## **B. INSTRUMENTATION**

Data acquired during the October experiment were collected from a 6m tower on the beach and instrument strings in the surf zone (see Figure 4). Instrument locations on the tower and specifications are given in Table 1. Wind speed and direction were measured using 3 dimensional ultrasonic anemometers placed at six evenly spaced intervals on the tower. Temperature and relative humidity were measured at the anemometer levels using an integrated probe system. Surface temperature was measured using a downward looking infrared radiometer and total radiation transfer was measured using a bi-directional net radiometer. The tower instruments were powered by one 12V marine battery that experienced some power degradation resulting in loss of data (see Table 1). All tower data were recorded on a CR6 measurement and control datalogger. The ocean temperature was measured using an array of thermistors at varying depths. However, due to the shallow depth of the location, the temperatures were nearly isothermal and were averaged for simplicity. Water level height was obtained from National Data Buoy Center station MTYC1 in 6-minute averages.



From bottom center clockwise, Apogee SI-111 PW Infrared Radiometer, RBR Solo-T Temperature Logger, RM Young Ultrasonic Anemometer Model 81000, CR6 measurement and control datalogger, Campbell Scientific HC253-L Temperature and Relative Humidity Probe, Kipp & Zonen CNR4 Net Radiometer. Sources: Campbell Scientific (b), RBR, Young, Campbell Scientific (a), Campbell Scientific (c), Kipp and Zonen.

Figure 4. Instruments and Tower Setup during the October Experiment

During CLASI, one 3-D ultrasonic anemometer and one temperature/relative humidity sensor were mounted on each of seven 6m towers and deployed along the shore of the Monterey Bay according to the configuration in Table 2. The battery packs on these towers were augmented with two battery recharging SP10 10 W solar panels to mitigate data loss.

Table 1. Instrumentation for October Deployment

Instrument	Sampling Rate	Level	% Loss
(6) RM Young Ultrasonic Anemometer Model 81000	20Hz	1	26.82
		2	20.03
		3	24.52
		4	22.02
		5	46.01
		6	45.89
(6) Campbell Scientific HC253-L Temperature and Relative Humidity Probe	1Hz	1	12.95
		2	11.91
		3	11.91
		4	11.91
		5	35.69
		6	35.69
(1) Apogee SI-111-PW Infrared Radiometer	1Hz	1.5	11.91
(1) Kipp & Zonen CNR4 Net Radiometer	1Hz	1.5	12.95
(1) RBR Solo-T Temperature Logger	1Hz	N/A	10.45

Levels given are 1) 1.19 m, 1.5) 1.69 m, 2) 2.19, 3) 3.19 m, 4) 4.19 m, 5) 5.19 m, 6) 6.19 m.

Table 2. Instrumentation for CLASI Deployment

Instrument	Sampling Rate	Location	% Loss
(7) RM Young Ultrasonic Anemometer Model 81000	20Hz	DMB1	17.5893
		DMB2	5.9226
		DMB3	6.1310
		ESN	1.1012
		ESS	1.1905
		MAB	1.2202
		MRB	1.2798
(7) Campbell Scientific HC253-L Temperature and Relative Humidity Probe	1Hz	DMB1	17.5893
		DMB2	5.9226
		DMB3	6.1310
		ESN	1.1012
		ESS	1.1905
		MAB	1.2202
		MRB	1.2798
(12) RBR Solo-T Temperature Logger	1Hz	ESN, ESS, MAB, MRB	0
(5) RBR Solo-D Pressure Logger	1Hz	ESN, ESS, MAB, MRB, DMB	0

Locations include MAN, ESN, ESS, MAB, DMB1, DMB2, DMB3.

### C. DATA PROCESSING

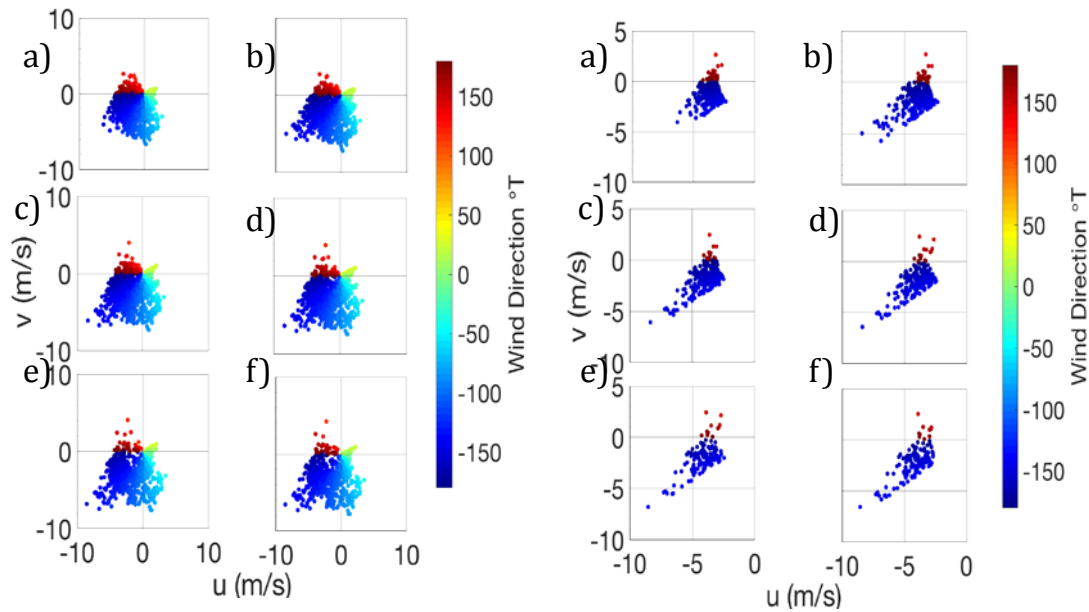
Raw data were processed according to the methods described by Aubinet et al. (2012), including despiking and cross-correlation of the time series data to align all signals to the same time base. Winds were rotated into a shore-normal frame of reference. All data outside of  $\pm 140^\circ$  T were filtered out to remove offshore winds and the influence of the instrument tower. Wind speeds less than 3 m/s were removed, as they were not considered to contribute significantly to atmospheric instability. Stability was then limited to  $-2 < \zeta < 0.5$  (October) and  $-5 < \zeta < 0.5$  (CLASI) for all calculations. Once preprocessing was complete, the data were compressed into 15-minute averages, wherever 15 full minutes of data were available.

THIS PAGE INTENTIONALLY LEFT BLANK

## IV. RESULTS

### A. ENVIRONMENT

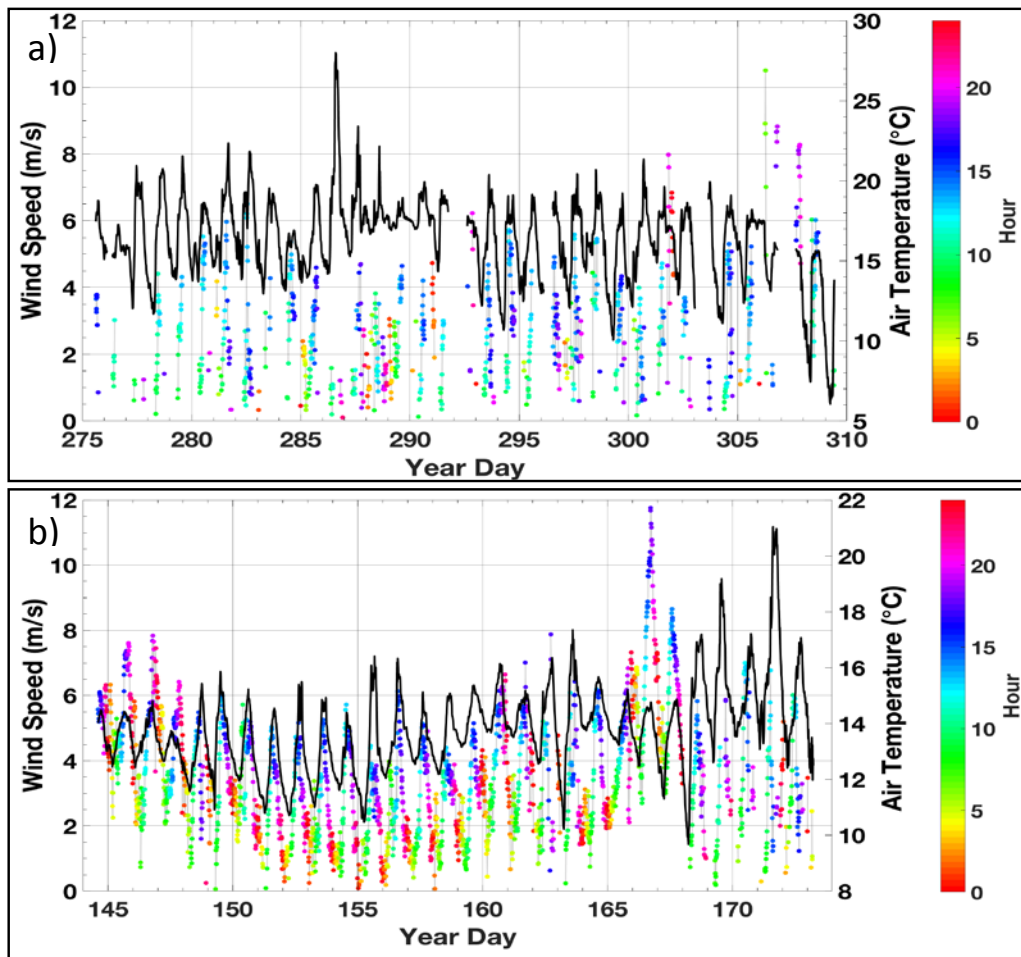
To understand the state of the environment during the two field experiments, various analyses of the data were performed. First, wind speed and direction were examined to determine the most appropriate ranges for use. The along-shore winds were plotted vs. cross-shore winds for the October experiment (see Figure 5). The lowest wind speeds (<3 m/s) and offshore winds, which are also generally lower, were not considered to be major contributors to heat flux and were removed (see Figure 5), this limitation was also applied to the CLASI data



Cross-shore ( $u$ ) winds plotted vs. along shore ( $v$ ) winds are color coded by wind direction. The plot on the left are the unconstrained data and the plot on the right are data that have been confined to speeds of  $>3$  m/s and wind direction between  $\pm 140^\circ\text{T}$ . Measurement height levels are a) 1.19 m, b) 2.19 m, c) 3.19 m, d) 4.19 m, e) 5.19 m, and f) 6.19 m.

Figure 5. Wind Speed vs. Direction

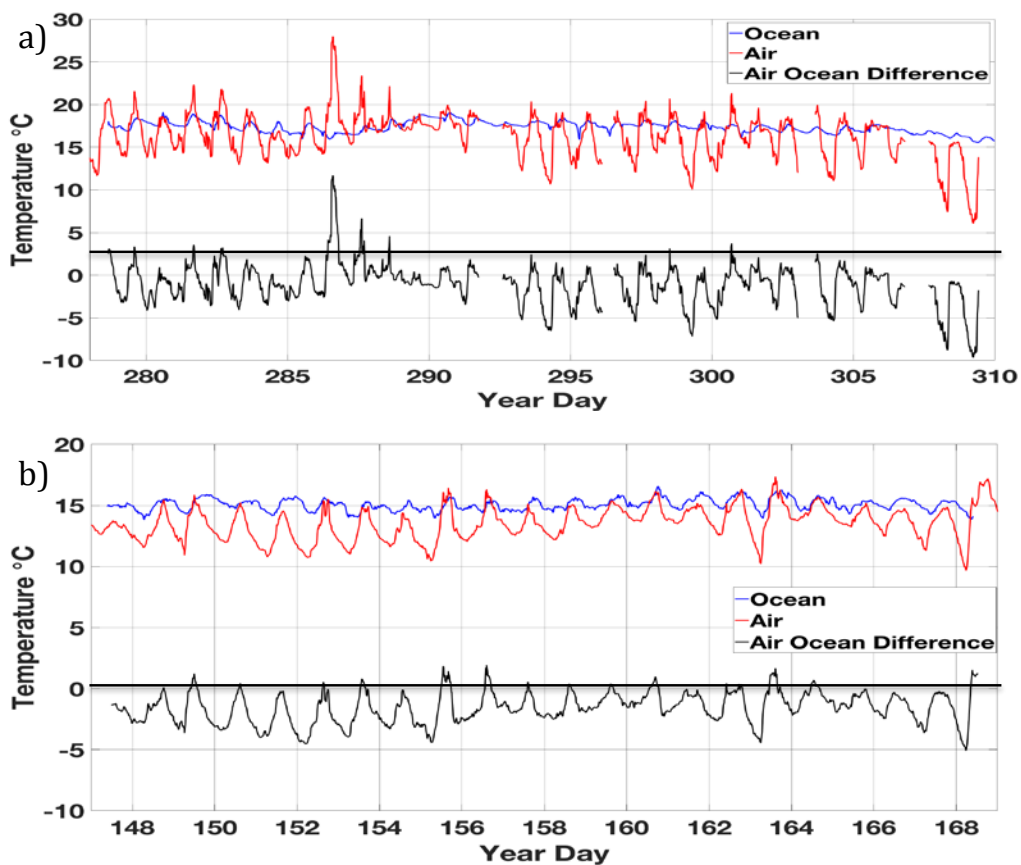
To find out when higher winds were occurring, temporal variations of the wind and temperature from the flux towers, averaged over all six height levels for the October experiment and over all seven locations for the CLASI experiment, were plotted (see Figure 6). Wind speed was color-coded by hour of the day and, for both experiments, the highest wind speeds occurred in the mid to late afternoon and corresponded to relatively warm temperatures (see Figure 6).



Time series of wind speed (colored dots) and air temperature (black line), averaged over all respective instruments for a) October and b) CLASI and color-coded by the hour of day.

Figure 6. Hourly Wind Speed and Air Temperature

Finally, using air temperature data from the towers, averaged as described above, and ocean temperature from the RBR Solo-T thermistors, averaged, the ocean and air temperatures were plotted in time series for both experiments (see Figure 7). The air-ocean temperature difference was plotted on the same figure to show that for over 90% of the CLASI experiment and over 65% of the October experiment, the ocean temperature was warmer than the air temperature (see Figure 7). This air-sea temperature difference indicates thermal instability and upward sensible heat flux from the ocean to the atmosphere.

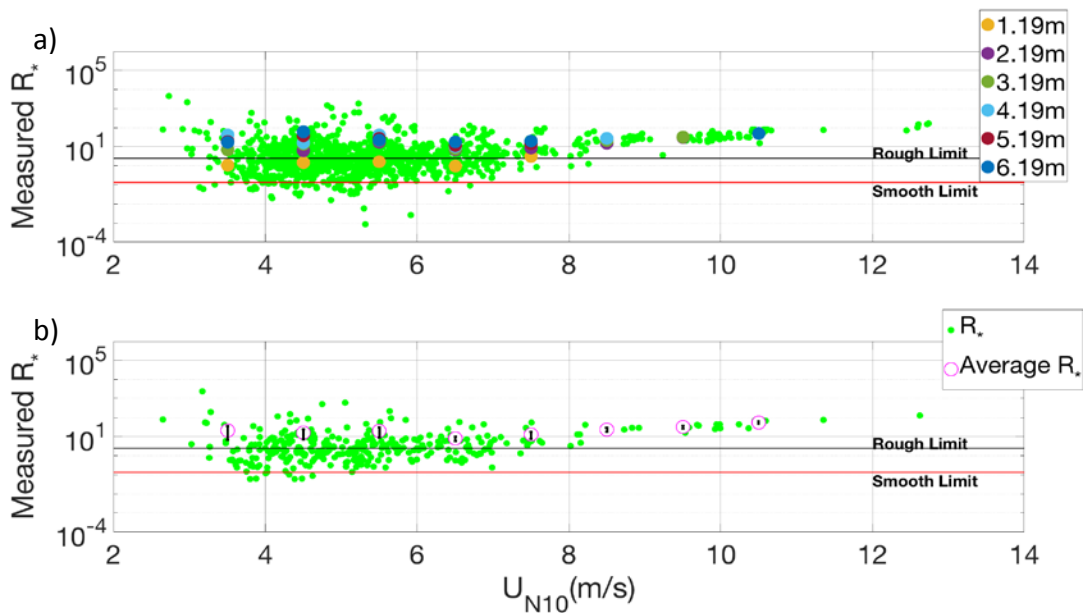


Averages of measured air and ocean temperatures are shown as the blue and red lines, the difference is shown in black and the black horizontal lines at zero are to show the cutoff for air warmer than ocean. The ocean is warmer than the air (a) 68.42% of the time for the October experiment and (b) 90.69% of the time for the CLASI experiment.

Figure 7. Air-Ocean Temperature Difference

## B. ROUGHNESS

As an initial estimate of the aerodynamic properties of our environment and following the methods of Andreas et al. (2012), Roughness Reynolds Numbers ( $R_*$ ) were calculated and plotted for each vertical level on the October tower (see Figure 8). Cutoffs for aerodynamically smooth flow at a value of 0.135 and aerodynamically rough flow at a value of 2.5 (Andreas et al. 2012) were used to separate the roughness regime of the flow. Very little of the data were below the smooth limit and in fact, 95.89% of the  $R_*$  values were in either the transitional or the rough regimes, and 53.36% were above the rough line and therefore in the aerodynamically rough regime.

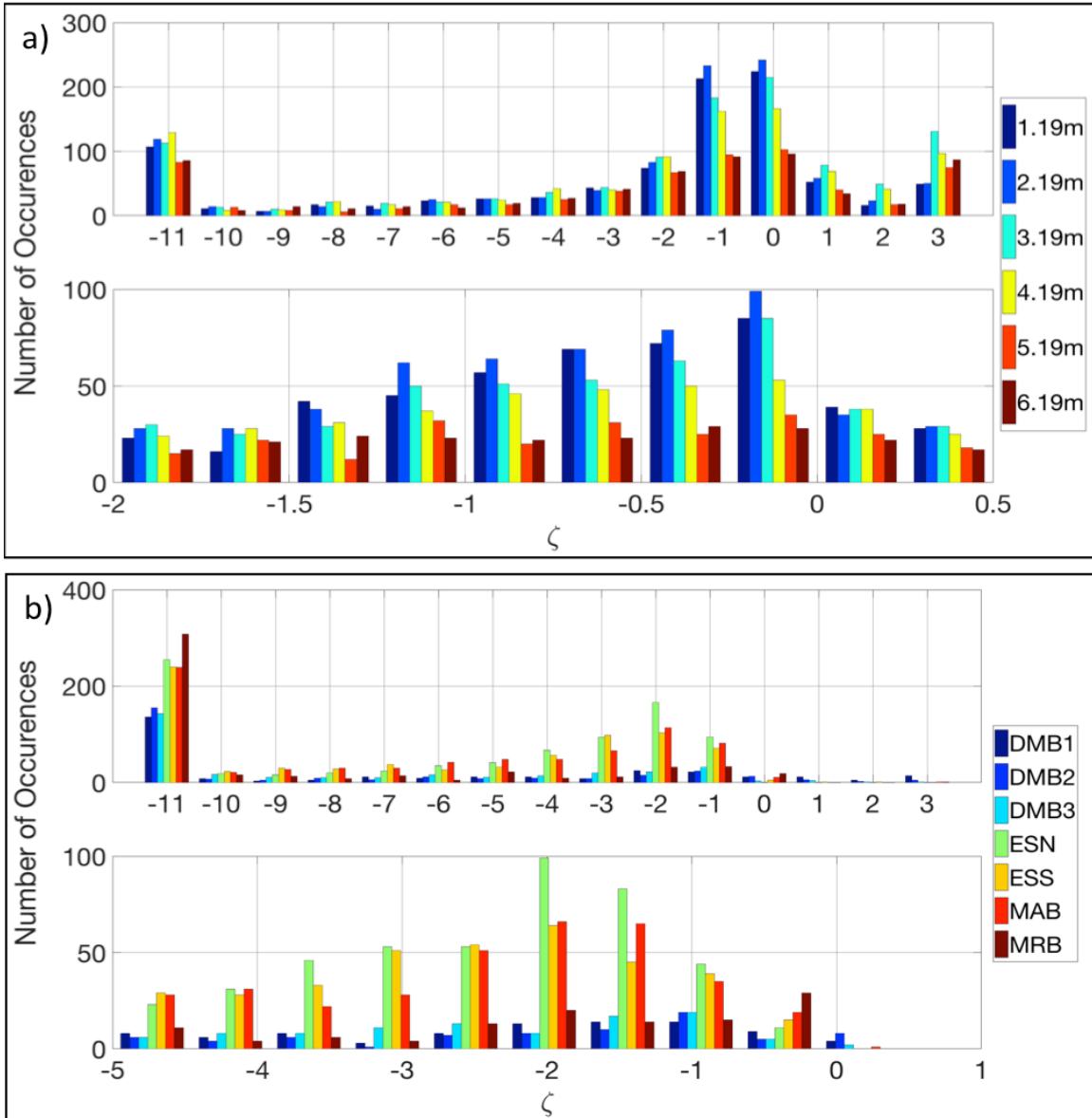


The horizontal lines show the aerodynamically smooth limit (at 0.135) and the aerodynamically rough limit (at 2.5) (Andreas et al. 2012). a) The colored circles are means at each level within  $U_{N10}$  in  $1 \text{ ms}^{-1}$  bins. b) The magenta circles are the average  $R_*$  for all levels within a bin the black bars are the 95% confidence interval.

Figure 8. Roughness Reynolds Number

### C. STABILITY

Expecting some instability in the atmosphere based on our environmental conditions, stability values for both experiments were calculated using the Monin-Obukhov parameter,  $\zeta$ , and analyzed using a histogram distribution. The range of stability that best represents our data set for the October experiment is  $-2 < \zeta < 0.5$  (see Figure 9a) and is increased to  $-5 < \zeta < 0.5$  for the CLASI experiment (see Figure 9b). The ranges confirm that the environment in both experiments was mildly unstable with CLASI being more unstable due to the more frequent occurrence of warm water under cool air.

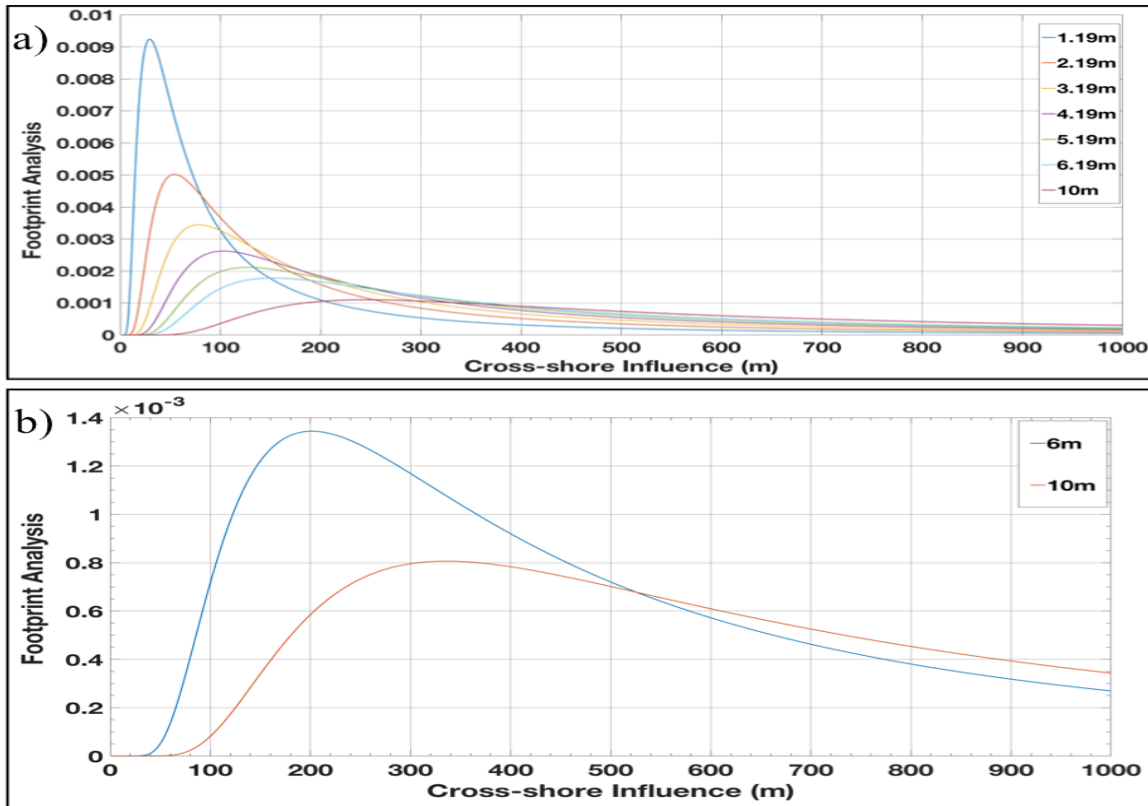


Histogram distribution of stability values ( $\zeta$ ) for a) October and b) CLASI. The top plot shows the total data set; the values at -11 and 3 include all points below or above them respectively. The bottom plot is the distribution of  $\zeta$  used in the analysis.

Figure 9. Thermal Stability

#### D. FOOTPRINT

Footprint analyses were conducted to identify the origin of the sampled turbulent eddies. This analysis was performed for the towers on Del Monte Beach including the October experiment, DMB1, DMB2 and DMB3. The probability density function curves of the footprint analysis for the six levels from 1.19 m to 6.19 m as well as a 10 m reference were plotted vs. the cross-shore influence, which is the distance seaward from the instrument tower (see Figure 10). The footprint analysis for the other CLASI towers (MAB, ESS, ESN and MRB) is closely represented by the 6.19m curve in Figure 10. This shows that for the lowest level, the area of origin begins very close to the tower but as the height increases, the area of origin moves offshore.



Probability distribution function of footprint analysis for a) October and b) CLASI vs. cross-shore influence, or distance seaward from the instrument at the origin.

Figure 10. Footprint Analysis

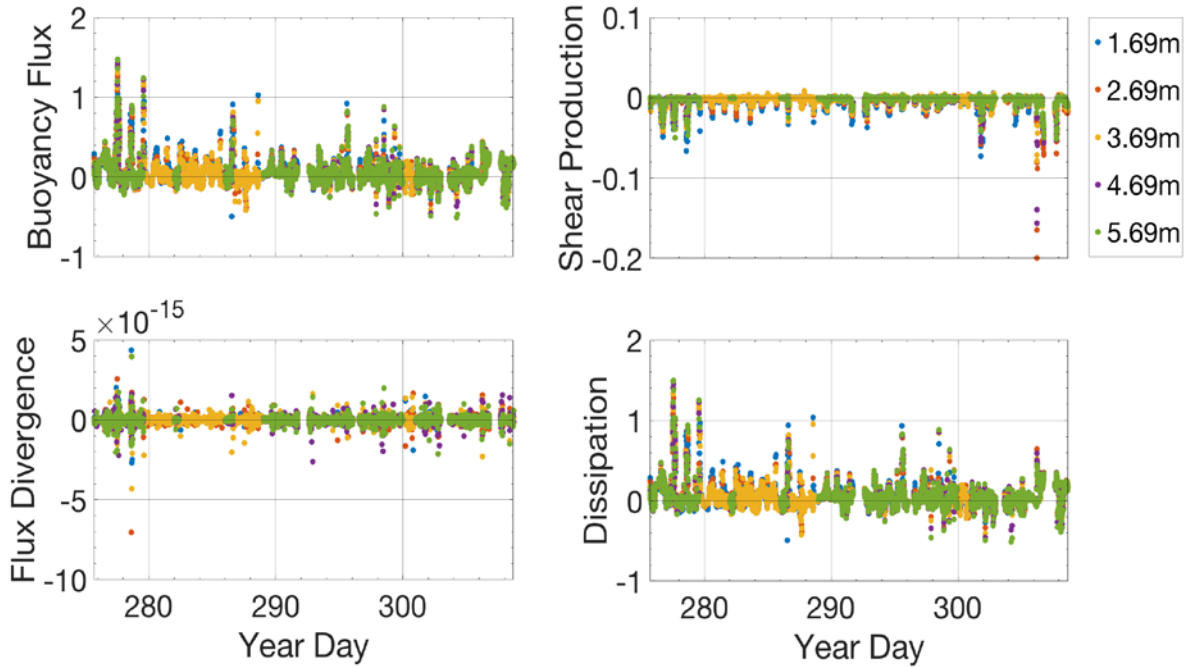
The footprint analysis was then used to separate the measured data into three zones including the sand, the surf zone and the area outside of the surf zone. A 70% cut off was chosen to separate the data into the zones. If 70% of the area under the footprint curve was inside one of those designated regions, the data were considered to have originated in that region; a process made more challenging by the changing tides. Data not falling into one of the three categories was kept for comparison.

## E. TURBULENCE KINETIC ENERGY

To determine the cause of turbulence in the environment during the experiments, turbulence kinetic energy budget terms was calculated by rearranging Equation (11):

$$\frac{g}{\theta_v}(\overline{w'\theta'_v}) - \overline{w'u'}\frac{\partial\bar{u}}{\partial z} - \frac{\partial(\overline{w'e})}{\partial z} = \varepsilon \quad (20)$$

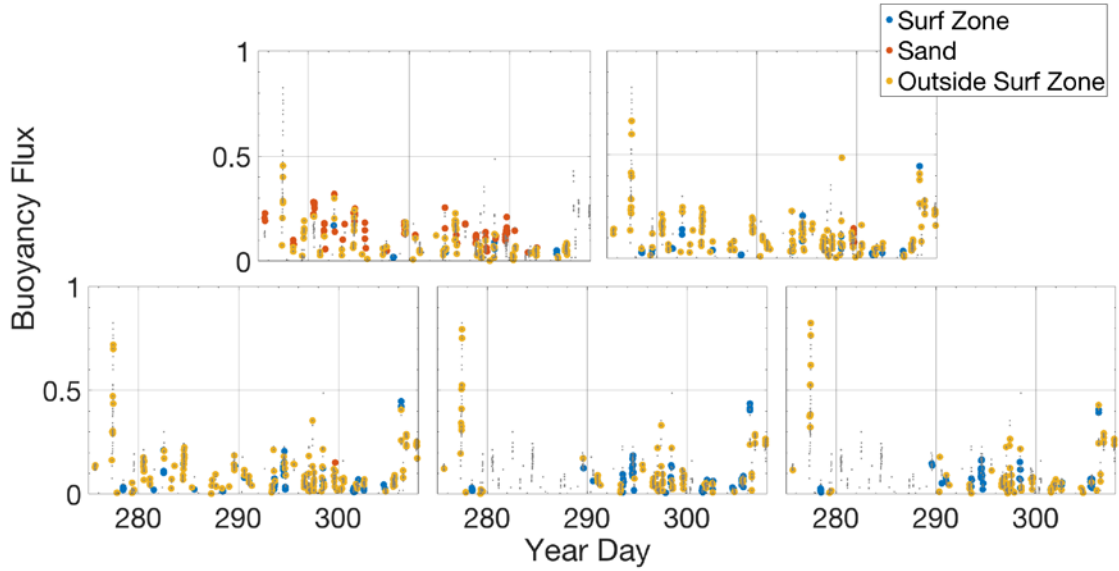
Now the three terms on the left, buoyancy flux, shear and flux divergence balance dissipation on the right. The buoyancy flux appears to be several orders of magnitude larger than both the shear production and the flux divergence, meaning that it is likely the primary balancing force to dissipation and therefore the main influence on TKE (see Figure 11). Due to the difficult nature of estimating wind shear, there is potential error in these calculations but there is reasonable confidence in the results. Because the calculations required two height levels, this method was not used for the CLASI experiment; results shown are for the October experiment.



The TKE budget, the four main terms are plotted in time series for the length of the October experiment.

Figure 11. The Terms of the TKE Budget

Buoyancy flux was separated into footprint-based contributions as previously described. Points that did not meet the 70% criteria were still considered in the overall buoyancy flux (see Figure 12). For the lowest level at 1.69 m, the sand is the highest contributor at 45%, vs. 29% surf and 26% ocean. For each of the other levels the surf zone is the highest contributor, 36% vs. 33% sand and 31% ocean at 2.69 m, 39% vs. 31% sand and 30% ocean at 3.69 m, 42% vs. 29% sand and 29% ocean for 4.69 m, and 40% vs. 29% sand and 31% ocean for 5.69 m (see Figure 13).



Buoyancy flux values are separated into their footprint based contributions from the sandy beach, the surf zone and the ocean outside of the surf zone. Levels from top left to bottom right are 1.69 m, 2.69 m, 3.69 m, 4.69 m and 5.69 m.

Figure 12. Zonally separated Buoyancy Flux

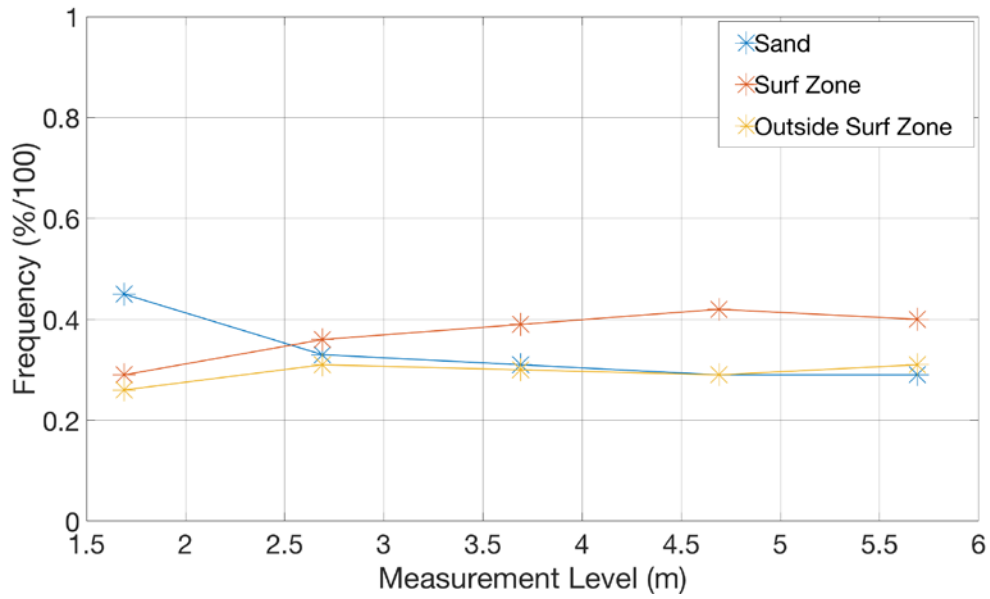


Figure 13. Contributions of Sand, Surf Zone and Ocean outside Surf Zone

## F. SENSIBLE HEAT FLUX

It was assumed that the initial droplet size was on the order of 0.16-47  $\mu\text{m}$  based on the findings of De Leeuw et al. (2000). Using that size range, sensible heat from the surf zone sea spray was calculated with the methods of Andreas et al. (2015), as:

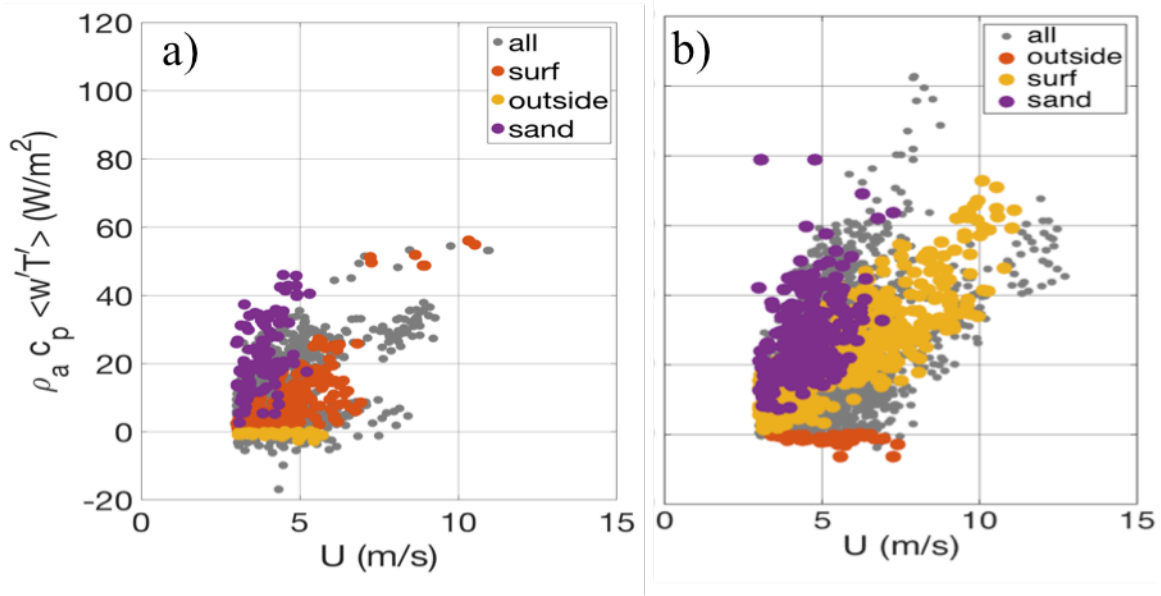
$$H_{L,sp} = \alpha \overline{H_L} \quad (21)$$

and

$$H_{S,sp} = \beta \overline{H_S} - (\alpha - \gamma) \overline{H_L}, \quad (22)$$

where  $\alpha$ ,  $\beta$  and  $\gamma$  are small turning coefficients, determined to be 2.46, 15.15 and 1.77 respectively (Andreas et al., 2015),  $\overline{H_L} = \int_{1.6}^{500} H_L(r_0) dr_0$  and  $\overline{H_S} = \int_{1.6}^{500} H_S(r_0) dr_0$  are the integrated latent and sensible heat exchanges (Andreas et al. 2016).

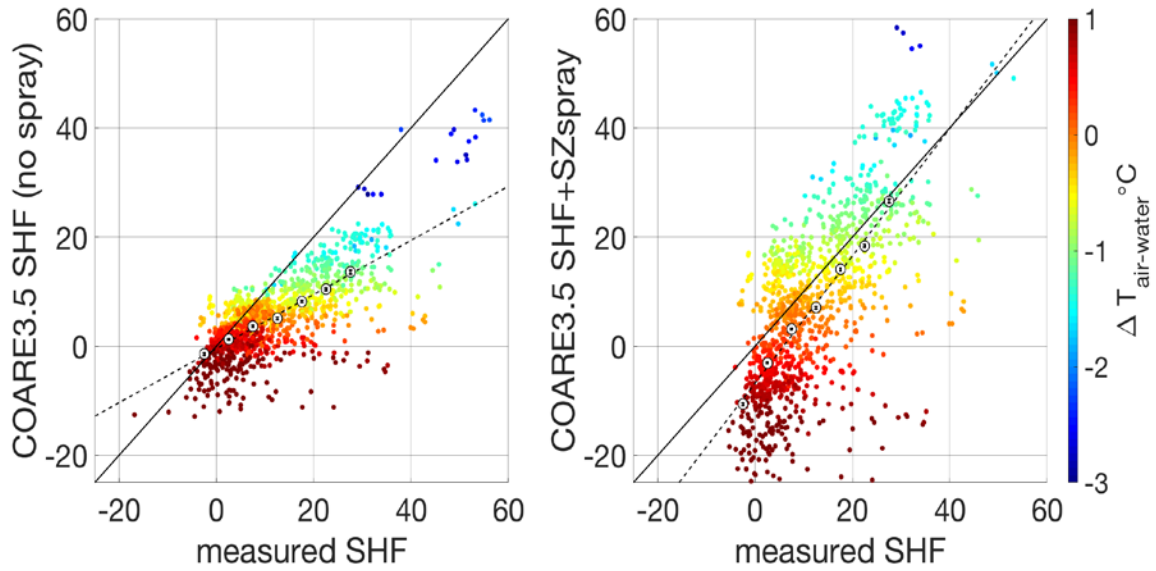
Calculated sensible heat values were separated into footprint-based zones in the manner described above. Points that did not meet the 70% criteria were still considered in the overall sensible heat flux. Measured and zoned sensible heat flux is plotted against wind speed for both the October and CLASI experiments (see Figure 14). In both cases, the sand contributed more sensible heat flux at low wind speeds. That is because the land is warmer than the ocean and at those lower wind speeds, the environment is more stable and the footprint is closer to the tower, therefore covering more of the sand than the surf zone. The sand contribution is overtaken by the contribution from the surf zone at higher wind speeds where instability has increased and the footprint has moved outward. Contributions from the area outside of the surf zone were close to zero because, in order for the sensors to receive measurements from that area, the environment would have to be much more stable. That stability would in turn decrease the amount of sensible heat flux available for measurement. In both cases, the measured sensible heat flux is greater than that predicted by the model.



Sensible heat flux separated into the contributions from the sand, the surf zone and outside the surf zone plotted vs. wind speed ( $U$ ) for a) October and b) CLASI.

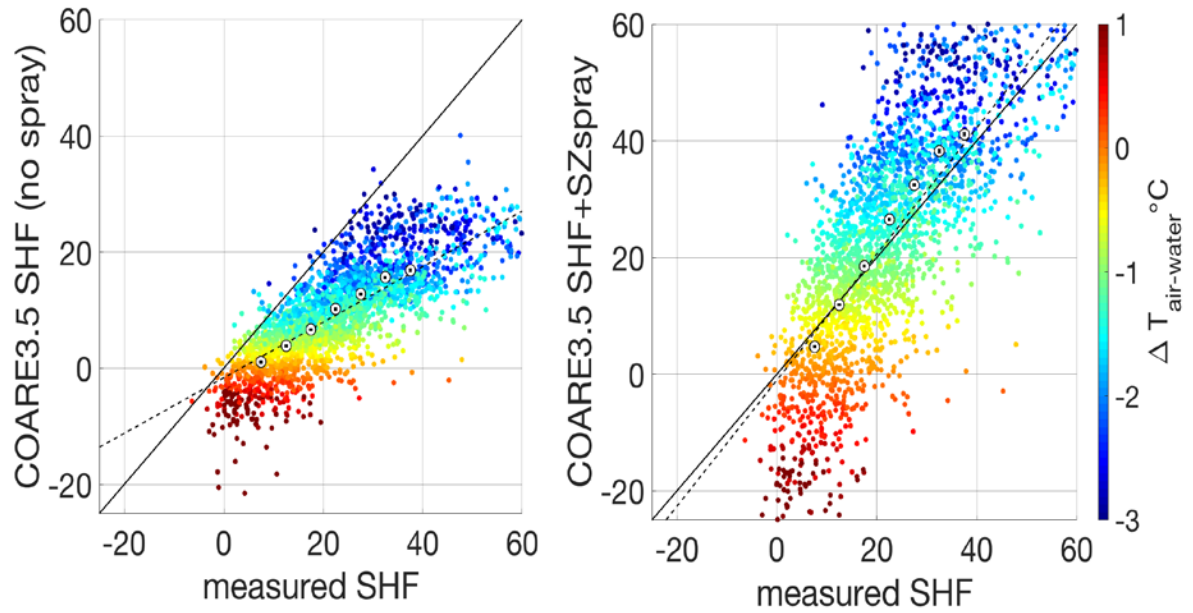
Figure 14. Sensible Heat Flux

Noting the large number of points in the surf zone for each experiment, sensible heat was again calculated using equations 4–11 to include the influence of sea spray. The results were plotted against the COARE 3.5 model calculations and color-coded based on the air-water temperature difference. The slopes of the linear regression lines, plotted for the October experiment data are 0.50 without sea spray and 1.16 with sea spray included (see Figure 15). For the CLASI experiment, the slopes of the linear regression lines were 0.48 without sea spray and 1.08 with spray included (see Figure 16). This means that the COARE 3.5 model, which is designed for the open ocean, is underestimating the sensible heat flux in the surf zone by over 50%. With the sea spray sensible heat flux included however, the estimate is much more accurate. The COARE 3.5 model was chosen for its ease of use and functionality. Other model results were not investigated in this effort but further comparisons would benefit this field of study.



Measured vs. modeled sensible heat flux without influence from sea spray on the right and with sea spray included on the left. The white circles represent the averages for  $5 \text{ Wm}^{-2}$  wide bins. The solid line is 1:1 and the dashed line is the linear regression. The slopes of the regression lines are 0.4957 with no spray and 1.16 with spray included.

Figure 15. Sensible Heat Flux from October Experiment



Measured vs. modeled sensible heat flux without influence from sea spray on the right and with sea spray included on the left. The solid line is 1:1 and the dashed line is the linear regression. The white circles represent the averages for 5  $\text{Wm}^{-2}$  wide bins. The slopes of the regression lines are 0.4784 with no spray and 1.08 with spray included

Figure 16. Sensible Heat Flux from CLASI Experiment

## V. SUMMARY AND CONCLUSIONS

Wind, temperature and relative humidity were measured along the coast of the Monterey Bay during two field experiments conducted in October 2015 and June 2016 (CLASI). In both experiments, the winds of interest were onshore from  $\pm 140^\circ T$ . The water temperature was warmer than the air temperature for 68.42% of the October experiment and 90.69% of the CLASI experiment suggesting thermal instability in the atmospheric surface layer during the experiment periods.

Using Reynolds Roughness number as a measure of surface roughness regimes, we found that the atmosphere was in a transient to rough regime for over 95% of the October experiment. Further analysis using the Monin-Obukhov stability parameter  $\zeta$  showed that the atmospheric surface layer was in the neutral to slightly unstable stability regime for both experiments.

Instability in the atmosphere, coupled with onshore winds created a footprint that allowed the instrument arrays to collect data originating in the sand, the surf zone and the area just beyond the surf zone. Sensible heat flux calculated directly from the data collected during the October and CLASI experiments was separated into its contributions from those zones and further confined based on wind speed and direction and atmospheric stability. The refined data were then compared to COARE 3.5 model estimate of sensible heat flux. The model under predicted sensible heat flux for the surf zone by over 50% for both experiments. It was believed that the missing sensible heat flux was a result of sea spray aerosols. While the size and volume flux of these aerosols are not known exactly, there are various estimates, as explained by Cavaleri et al. (2012).

There is strong uncertainty about the actual global production of sea-spray aerosols. The present estimates (see de Leeuw et al. 2011) span two orders of magnitude, between 0.02 and  $1 \text{ Å} \sim 10^{14} \text{ kg yr}^{-1}$ , of whose small range ( $< 1 \text{ μ m}$ ), 20% or more, is expected to be organic matter. As breaking waves are especially abundant in the surf zone, Monahan (1995) speculated that many more sea-spray aerosols per unit area and time would be generated over the surf zone than in the open ocean, and these have been observed to be transported over tens of kilometers. (Cavaleri et al. 2012)

Knowing that there is a large amount of sea spray in the surf zone, the sea spray sensible heat flux was added to the model estimate of sensible heat flux. With that addition, the calculated total sensible heat flux (interfacial and sea spray heat fluxes) compared much better with observations with the estimated values being slightly larger. The assumptions made during this analysis may involve some uncertainties due to the lack of sea spray measurements. However, the results are qualitatively informative.

Sensible heat flux from sea spray aerosols significantly increases the total sensible heat flux in the surf zone and therefore cannot be ignored when parameterizing sensible heat in numerical modeling. In this set of experiments, only the 70% footprint coverage was considered but other distributions should be explored for completeness. This effort focused on the surf zone but the footprint area could be moved or expanded based on different stability and height factors to examine other parts of the coastal environment.

## LIST OF REFERENCES

- Akylas, E. and Tombrou, M., 2005: Interpolation between Businger-Dyer formulae and free convection forms: A revised approach. *Boundary-Layer Meteorology*, 115, 381–398, doi:10.1007/s10546-004-1426-3.
- American Meteorological Society, 2017: Reynolds Number. Glossary of Meteorology: Accessed 2 March, 2017 [Available online at <http://glossary.ametsoc.org/wiki/ReynoldsNumber>.]
- Andreas, E.L., 1992: Sea spray and the turbulent air-sea fluxes. *J. of Geophysical Research*, 97, 11,429-11,441.
- Andreas, E.L., 2016: Sea spray generation at a rocky shoreline. *Amer. Meteor. Society*, 55, 2037–2052, doi:10.1175/JAMC-D-15-0211.1.
- Andreas, E.L., Mahrt, L., Vickers, D., 2012. A new drag relation for aerodynamically rough flow over the ocean. *Journal of Atmospheric Sciences*, 69, 2520–2537.
- Andreas, E.L., Mahrt, L., Vickers, D., 2015: An improved bulk air-sea surface flux algorithm, including spray-mediated transfer. *Quart. J. of the Roy. Meteor. Soc.*, 141, 642–654, doi: 10.1002/qj.2424.
- Aubinet, M., T. Vesala, D. Papale, 2012: Eddy covariance: A practical guide to measurement and data analysis. Springer Science & Business Media, 451pp.
- Campbell Scientific: CR6 Data logger (a), 2017: Accessed 5 January, 2017 [Available online at <https://www.campbellsci.com/cr6>.]
- Campbell Scientific: Infrared Radiometer with Standard Field of View(b), 2017: Accessed January 5, 2017 [Available online at <https://www.campbellsci.com/si-111>.]
- Campbell Scientific: HC2S3-L Temperature and Relative Humidity Probe (c), 2017: Accessed 5 January 2017 [<https://www.campbellsci.com/hc2s3>.]
- Chomka, M. and Petelski, T., 1997: Modeling the sea aerosol emission in the coastal zone. *Oceanologia*, 39, 211–225.
- De Leeuw, G., Neele, F.P., Hill, M., Smith, M.H., Vignati, E., 2000: Production of sea spray aerosol in the surf zone. *J. of Geophysical Research*, 105, D24, 29,397-29,409.
- Garratt, J.R., 1992: The atmospheric boundary layer. Cambridge University Press, 316pp.

- Hohenstein, C.G., Jaeger, J.W., Jones, D.L., 1965: A study of marked sand movement on Del Monte Beach, Monterey Bay, California. M.S. thesis, Dept. of Oceanography, Naval Postgraduate School, 291 pp.
- Kipp & Zonen. CNR4 Net Radiometer, 2017: Accessed 5 January 2017 [Available online at <http://www.kippzonen.com/Product/85/CNR4-Net-Radiometer-.WSS6P1LMxBw.>]
- Mahrt, L., Vickers, D., Andreas, E.L., Khelif, D., 2012: Sensible heat flux in near-neutral conditions over the sea. *Journal of Physical Oceanography*, 42, 1134–1142, doi: 10.1175/JPO-D-11-0186.1.
- Neele, F.P., de Leeuw, G., Martijn, J., Stive, M., 1998: Quantitative assessment of surf-produced sea spray aerosol. SPIE Conference on Propagation and Imaging through the Atmosphere II, San Diego, CA, July 1998, SPIE Vol 3433.
- Nilsson, E., Lohou, F., Lothon, M., Parkyjak, E., Mahrt, L., Darbieu, C., 2015: Turbulence kinetic energy budget during the afternoon transition-Part1: Observed surface TKE budget and boundary layer description for 10 intensive observation period days. *Atmospheric Chemistry and Physics*, 16, 8849–8872, doi: 10.5194/acp-16-8849-2016.
- Peel, M.C., Finlayson, B.L, McMahon, T.A., 2007: Updated world map of the Köppen-Geiger Climate Classification. *Hydrology and Earth System Sciences*, 11, 1633–1644.
- Pond, S., Phelps, G.T., Paquin, J.E., McBean, G., Stewart, R.W., 1971: Measurements of the turbulent fluxes of momentum, moisture and sensible heat over the ocean. *J. Atmos. Sci.*, 28, 901–917.
- RBR: RBRsolo T | Temperature Logger, 2017: Accessed 5 January 2017 [Available online at <https://rbr-global.com/products/compact-loggers/rbrsolo-t.>]
- Shabani, B., Babanin, A.V., Baldock, T.E., 2016: Observations of the directional distribution of the wind energy input function over swell waves. *Journal of Geophysical Research: Oceans*, doi:10.1002/2015JC011225.
- Srivastava, M.K. and Sarthi, P.P., 2002: Turbulent kinetic energy in the atmospheric surface layer during the summer monsoon. *Meteorological Applications*, 9, 239–246, doi:10.1017/S1350482702002098.
- Stull, R.B., 1988: *An Introduction to boundary layer meteorology*. Kluwer Academic Publishers, 666pp.

- Van Eijk, A.M.J., Kusmierczyk-Michulec, J.T., Francius, M.J., Tedeschi, G., Piazzola, J., Merritt, D.L., Fontana, J.D., 2011: Sea-spray aerosol particles generated in the surf zone. *Journal of Geophysical Research*, 116, D19210, doi: 10.1029/2011JD015602.
- Vego, M., 2014: On littoral warfare. *Naval War College Review*, Spring 2015. Vol 68, No. 2.
- Vickers, D., Mahrt, L., and Andreas, E.L., 2013: Estimates of the 10-m neutral sea surface drag coefficient from aircraft eddy-covariance measurements. *Journal of Physical Oceanography*, 43, 301–310.
- Young: Ultrasonic Anemometer, 2017: Accessed 5 January 2017. [Available online at <http://www.youngusa.com/products/11/3.html>.]

THIS PAGE INTENTIONALLY LEFT BLANK

## **INITIAL DISTRIBUTION LIST**

1. Defense Technical Information Center  
Ft. Belvoir, Virginia
2. Dudley Knox Library  
Naval Postgraduate School  
Monterey, California